J. Synchrotron Rad. (1996). **3**, 112–119

Observation and Modelling of Preferred Orientation in Two-Dimensional Powder Patterns

N. G. Wright,† R. J. Nelmes, S. A. Belmonte and M. I. McMahon

Department of Physics and Astronomy, The University of Edinburgh, Edinburgh EH9 3JZ, UK

(*Received 27 January 1996; accepted 12 March 1996*)

A novel approach to the detection and modelling of preferred orientation is presented, based on the interpretation of two-dimensional powder patterns. A simple graphical construction is introduced to aid interpretation, and the application of this construction to some standard diffraction geometries is discussed. It is also shown in outline how a standard preferred-orientation model can be adapted to describe two-dimensional data.

Keywords: preferred orientation; powder diffraction; area detectors; two-dimensional data.

1. Introduction

Preferred orientation of sample crystallites has long been one of the most studied aspects of powder diffraction. In some fields, notably metallurgy (Barrett & Massalski, 1992), the emphasis has been on studying samples of known structure and extensive techniques have been developed to determine the crystallite orientation distribution from the observed diffraction patterns, collected from many sample orientations (Järvinen, Merisalo, Pesonen & Inkinen, 1970; Bunge, Dahms & Brokmeier, 1989; Dahms & Bunge, 1989). In powder diffraction studies performed to determine crystal structures (normally from data obtained using one sample orientation), preferred orientation is often modelled during structure refinement by using a simple analytic function (Rietveld, 1969; Capkova & Valvoda, 1974; Dollase, 1986). However, such a method presupposes that an approximate trial structure is known and this is clearly not the case during structure solution. Strong preferred orientation can be a serious stumbling block in structure solution from powder diffraction data because of large differences between observed and true reflection intensities. Even if the general arrangement of the structure is known, structural variables can be strongly biased by correlations with a preferred-orientation model selected simply on the basis that it appears to improve the fit to the data.

If the proportion of crystallites contributing to each reflection can be determined experimentally, however, then the reflection intensities can be corrected reliably and structure solution and refinement can proceed without uncertainties. Recent developments in texture analysis have highlighted the importance of this direct approach and outlined possible techniques using conventional one-dimensional data-collection methods (Järvinen, 1993; Cerny, Valvoda & Chladek, 1995; Peschar & Schenk, 1995). Unfortunately, the collection of the large amount of data required in such an approach is difficult and time-consuming with a conventional scanning detector, and this is a significant impediment. However, the problem can be overcome with the large-area two-dimensional X-ray detectors, such as image plates, that have been developed over the past few years for high-pressure powder diffraction (see Nelmes & McMahon, 1994). By collecting a whole diffraction pattern of complete powder rings in parallel, a large amount of additional information is recorded in a remarkably short time. It so happens that high-pressure conditions often cause rather pronounced preferred orientation in samples, and it is this convergence of a well adapted detector with strong effects that has stimulated our texture studies (Wright, 1995). However, the results are in no way limited to high-pressure applications, and can be expected to be of wide use in all powder diffraction work.

In this paper we illustrate the nature of two-dimensional data and introduce a simple graphical construction that gives a straightforward interpretation of the relationship between the data and the underlying preferred-orientation distribution. We show how a standard preferred-orientation model can be adapted to describe the two-dimensional data and we outline the application and possible benefits of this approach for some standard diffraction geometries.

2. Preferred-orientation effects in two dimensions

Fig. 1 shows two-dimensional diffraction patterns obtained from the same sample of precompressed HgS in two different orientations with respect to the incident X-ray beam. These patterns were collected on station 9.1 at SRS, Daresbury, using an image-plate detector and an X-ray wavelength of ~0.45 Å. The diffraction pattern of Fig. 1(*a*) was collected with the incident beam striking the sample along the axis of symmetry of the crystallite distribution, and the recorded intensities are uniform around the powder

† Now at Department of Electrical and Electronic Engineering, Merz Court, The University of Newcastle upon Tyne, Newcastle NE1 7RU, UK.

rings. In this case, the effects of preferred orientation manifest themselves only in departures of the relative reflection intensities from the ideal values corresponding to the crystal structure of the sample. Fig. 1(*b*) was collected with the distribution axis inclined at 50° to the incident beam, and clear variations in intensity can be seen around the powder rings. It is these intensity variations that contain the information required to define the preferred-orientation distribution in the sample without any knowledge of the crystal structure other than the unit cell. We will first show this qualitatively and then, in the next section, develop a quantitative model.

For simplicity, the distribution of crystallite orientations can be taken to be uniaxial and axially symmetric. Indeed, many samples have such a distribution, as shown by the axial symmetry of Fig. 1(*a*). (More complex distributions can, in principle, be treated by extensions of the same procedures as apply to this simple case.) A symmetric uniaxial distribution can be represented by contours on a spherical surface, as drawn schematically in Fig. 2, where values of the contours are shown decreasing from 4 at the poles to 1 at the equator. In a sample that exhibits preferred orientation, a particular crystallographic direction in each crystallite (the preferred-orientation *direction*, POD) tends to align along the axis of the distribution (the preferred-orientation *axis*, POA). [For example, for a sample with hexagonal symmetry and the unique axis taken along **c**, pressed into a flat-plate container, the POD is likely to be [001] with the POA normal to the flat plate.] Consider a particular crystallite, typical of the sample, as shown in

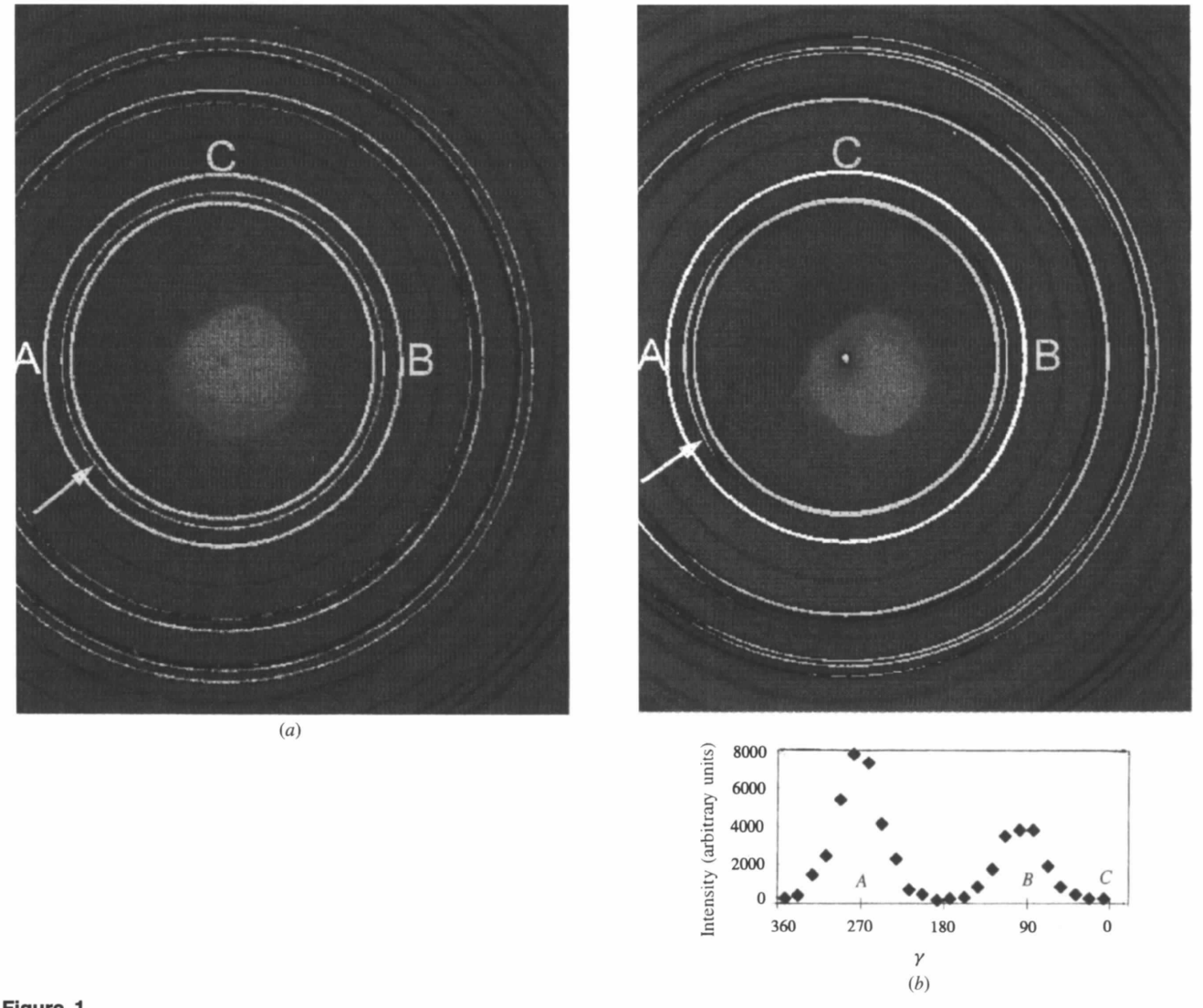

Figure 1
Two-dimensional diffraction patterns collected from the same HgS sample with (*a*) the axis of the crystallite distribution coincident with the incident X-ray beam, and (*b*) the axis of the crystallite distribution inclined at 50° to the incident beam. Note the intensity variations around the powder rings in (*b*). The ring of the (003) reflection is marked by an arrow in both patterns, and the plot of intensity *versus* γ (°) shows the variation of intensity for this reflection in pattern (*b*). γ is the angle around the powder ring (see Fig. 4). [The sense of the γ axis has been chosen to remain consistent with Fig. 4 while keeping the larger maximum (at *A*) to the left of the smaller, as in pattern (*b*).] The letters *A*, *B* and *C* mark the same positions around γ as illustrated in Fig. 3.

Fig. 2(*a*). Suppose that it is approximately shaped like a disc – viewed edge-on in the Figure – and that the POD is perpendicular to the plane of the disc. Such a crystallite in a general orientation has its POD at an angle α to the POA (see Fig. 2*a*), and the contours quantify how the relative probability of the POD being inclined at a given angle decreases as α increases.

Consider an incident beam direction labelled IB in Fig. 2(*a*), and the diffracted beam direction, DB, for reflection *hkl*. Suppose that the crystallite shown in Fig. 2(*a*) contributes to DB. The scattering vector $\mathbf{K}_{hkl}$ then bisects the angle between IB and DB, and $\mathbf{K}_{hkl}$ is at an angle ψ to the POD, where ψ is determined by the lattice parameters of the sample. However, *all* crystallites with their scattering vectors along the $\mathbf{K}_{hkl}$ direction will contribute to DB, and this family of crystallites is defined as all those with PODs lying on the cone shown in Fig. 2(*a*), with half-angle ψ around the $\mathbf{K}_{hkl}$. Thus, the probability of crystallites being oriented such as to contribute to the *hkl* reflection in direction DB is obtained as an integration of the distribution function around the circle where the POD cone intersects the surface of the sphere.

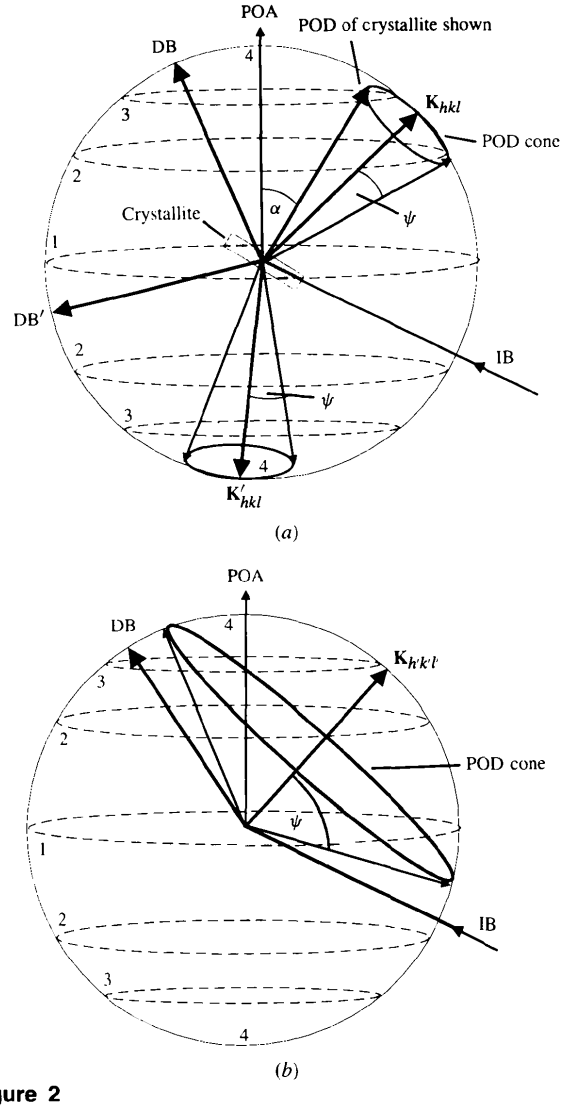

Figure 2
A uniaxial probability distribution function for crystallite orientations (ODF) can be represented as a series of contours on a unit sphere; the numbers 1 to 4 represent the value of the contours. (*a*) The POD cones for two points, DB and DB′, on the powder ring for reflection *hkl* when the incident beam (IB) strikes the crystallite distribution at an angle to the POA. A typical crystallite is shown, with its POD inclined at an angle α to the POA. (*b*) The POD cone for one point on a powder ring for a reflection, $h'k'l'$, with a large ψ angle.

Consider now another point on the *hkl* powder ring, given by DB′. The particular crystallite drawn in Fig. 2(*a*) will not contribute to this diffracted beam; DB′ is made up from reflections from another family of crystallites with PODs lying on the POD cone shown around $\mathbf{K}'_{hkl}$. It is immediately evident that the integrated probability is higher for this POD cone: more crystallites will contribute to DB′ than to DB and so the intensity of DB′ will be greater than that of DB. This difference is the source of the intensity variations around the powder rings in Fig. 1(*b*).

In the particular case drawn in Fig. 2(*a*), where ψ is small, the average of the integrated probability around the POD cone will be similar to the probability at the point where $\mathbf{K}_{hkl}$ passes through the surface of the sphere. Then the variation of intensity around the powder ring approximately gives a direct measure of the variation in the orientation distribution function (ODF) around the locus explored by all the *hkl* scattering vectors from $\mathbf{K}_{hkl}$ to $\mathbf{K}'_{hkl}$. However, it is important to note that the relationship between the ODF and the intensity variations is not so simple in general. Fig. 2(*b*) shows a POD cone for a different reflection, $h'k'l'$, with a large value of ψ. It is clear that the average of the integrated probability will differ from that for the single direction $\mathbf{K}_{h'k'l'}$ by an amount that depends on the form of the ODF.

The above discussion has illustrated some of the main two-dimensional effects of preferred orientation. In subsequent sections, we wish to analyse the effects of preferred orientation in more detail for a general diffraction geometry and for particular geometries in common use. In order to represent adequately the two-dimensional effects involved, it is helpful to consider three points (at least) in the diffraction pattern. A convenient form of construction for general use is then as shown in Fig. 3: three POD cones, separated by 90° in γ (see Fig. 1), and with a small ψ angle.

Fig. 3(*a*) shows a three-cone diagram for the setting in which the incident beam strikes the crystallite direction such that the POA coincides with the incident beam. The contours intersected by the POD cones can be seen to be identical in all three positions and consequently the intensity is the same at these three (and all other) points on the powder ring – *i.e.* the intensity around any powder ring is uniform – ignoring other possible effects such as polarization of the incident beam. This is the case illustrated by the two-dimensional image of Fig. 1(*a*), in which the positions around γ labelled *A* (270°), *B* (90°) and *C* (0°) correspond to the directions of DB(*A*), DB(*B*) and DB(*C*), respectively.

Fig. 3(*b*) is the diagram for a setting in which the incident beam strikes the sample at an angle β to the POA. The contours intersected by the three POD cones can be seen to represent different probabilities, and it is this effect that creates the pattern of intensity variation seen in Fig. 1(*b*). The angle β in Fig. 3(*b*) is 50°, as used in recording this image, and the arrowed powder ring in Fig. 1(*b*) has a small POD cone angle, as here. The POD cones for points *A* and *B* intersect contours of higher value than those for point *C* which will thus be an intensity minimum, as seen in Fig. 1(*b*). It is evident that the contours of the POD cone for point *A* are of higher value than those for point *B*, with the result that the maxima do not have the same intensity,

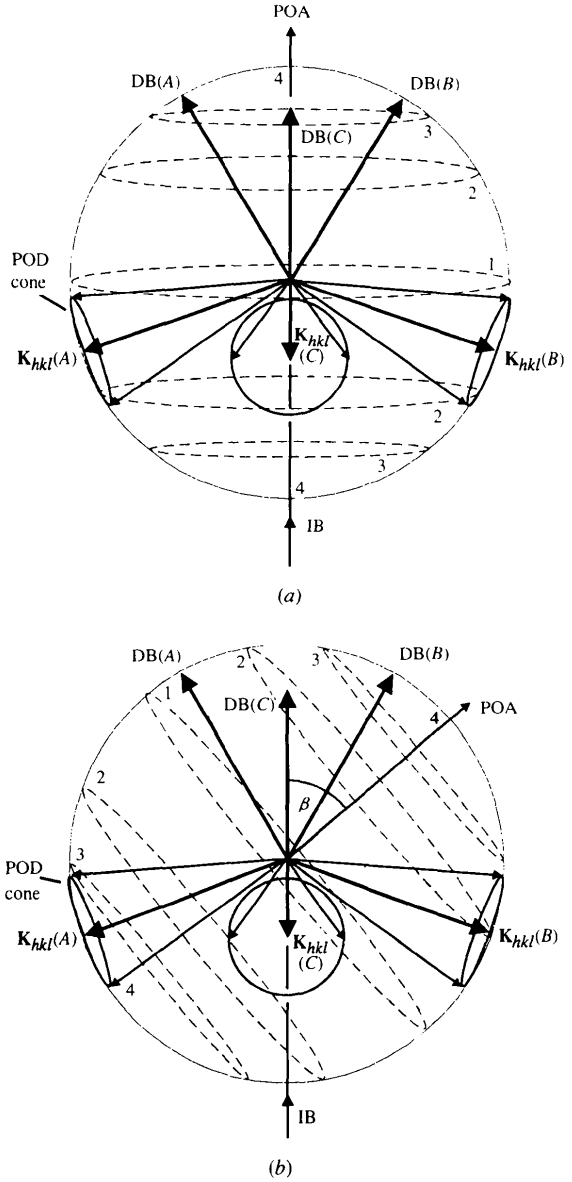

Figure 3
POD cone diagrams for diffraction at the three marked positions in γ (*A*, *B* and *C*) around the arrowed ring in (*a*) Fig. 1(*a*), and (*b*) Fig. 1(*b*). The angle between the POA and IB in (*b*) is labelled β. $\mathbf{K}_{hkl}(C)$ and DB(*C*) are directed upwards out of the plane of the diagram.

which accounts for the variation seen in the plot of intensity *versus* γ in Fig. 1(*b*). This asymmetry arises because the POD cone axes ($\mathbf{K}_{hkl}$) are not perpendicular to the incident beam, but are rotated away from perpendicular through the diffraction angle, θ. Thus, the asymmetry between the two maxima will increase with diffraction angle for a given angle β between the incident beam and the POA – until the cone axis of the larger maximum [$\mathbf{K}_{hkl}(A)$ in this case] reaches the maximum of the ODF.

It must be noted that another reflection, at similar θ but with a much larger POD-cone angle (ψ), would have its maxima and minima at different γ values from those of the particular reflection examined in Figs. 3(*b*) and 1(*b*). For example, if the POD-cone angle were increased greatly in Fig. 3(*b*), it can be seen that the average contour levels explored around a scattering vector near $\mathbf{K}_{hkl}(A)$ would decrease, while those explored around a vector near $\mathbf{K}_{hkl}(C)$ would (on average) increase. The variation in the γ angles at which different powder rings have their maxima and minima is evident in Fig. 1(*b*).

It is also important to stress that the foregoing analysis of intensity variations applies to single unoverlapped reflections – *e.g.* the (001) reflection of a tetragonal sample in which the *c* lattice parameter is sufficiently different from *a* (= *b*) to separate the (001) peak from the (100)/(010) peak. For a compound peak, like the latter one, the nature of the intensity variations will depend on the direction of the POD. If in this tetragonal example the POD is along [001], then ψ will be 90° for both (100) and (010) and so they will have identical variations as a function of γ. But, if the POD is along *e.g.* [100], then ψ will be 0° for (100) and 90° for (010), and their intensity variations will be 90° out of phase in γ; the maxima of the variations for (100) will coincide with the minima for (010), and so the observed variations around the (100)/(010) ring may be small even if the preferred-orientation effects are large. The intensity will not be uniform, however, and information about the ODF can still be extracted from such compound rings; but analysis of non-compound rings is considerably more straightforward. The overlap of symmetry-related reflections in preferred-orientation analysis has been discussed recently by Capkova, Peschar & Schenk (1993). In practice, there will also be similar problems for non-symmetry-related reflections if they are close enough in *d* spacing to overlap in the observed powder pattern. The HgS ring selected for analysis in Figs. 1 and 3 is the (003) reflection from a sample with hexagonal symmetry, and is not overlapped by symmetry-related or any other reflections, other than trivially by $(00\bar{3})$.

3. Preferred-orientation model

The qualitative discussion above provides a basis for understanding the effects of preferred orientation on a two-dimensional diffraction pattern. This section develops a mathematical model which can be used to extract the degree of sample texture quantitatively and thus correct the

reflection intensities for the effects of preferred orientation. Fig. 4(*a*) shows the orientation of the incident beam (IB), diffracted beam (DB) and scattering vector ($\mathbf{K}_{hkl}$) for diffraction at a given point on a diffraction pattern collected in a general scattering geometry. The z axis is set along the incident beam, which is usually horizontal, with x and y then vertical and horizontal, respectively, in the experimental set-up. Let θ be the scattering angle as defined by Bragg's Law, and γ be the angle between the x axis and the projection of both DB and $\mathbf{K}_{hkl}$ onto the xy plane [shown shaded in Fig. 4(*a*)]. If the two-dimensional detector is placed in the xy plane, γ corresponds to the angle around the powder rings; when $\gamma = 0°$, the diffracted beam and the scattering vector are in the (vertical) xz plane. (Point C in Fig. 1 is at $\gamma = 0°$.) Fig. 4(*b*) shows the cone of POD vectors for all the crystallites in the sample that are contributing to the *hkl* reflection in the selected direction.

The orientation of the POA with respect to the incident beam can be described in terms of the spherical polar coordinates, β and φ, of Fig. 4(*c*) as

$$\mathbf{POA} = \mathbf{a}\sin(\beta)\cos(\varphi) + \mathbf{b}\sin(\beta)\sin(\varphi) + \mathbf{c}\cos(\beta), \quad (1)$$

where (**a**, **b**, **c**) are unit vectors in the (x, y, z) directions. Expressing the POD vectors in terms of the coordinate axes of Fig. 4 is not trivial. However, by transforming to other coordinate axes, it can be shown (Wright, 1995) that the POD vector of a given diffracting crystallite can be expressed in terms of the (x, y, z) axes of Fig. 4 as

$$\begin{aligned}\mathbf{POD} = \mathbf{a}[&-\sin(\gamma)\sin(\psi)\cos(\delta)\\ &+ \sin(\theta)\cos(\gamma)\sin(\psi)\sin(\delta)\\ &+ \cos(\theta)\cos(\gamma)\cos(\psi)]\\ &+ \mathbf{b}[\cos(\gamma)\sin(\psi)\cos(\delta)\\ &+ \sin(\theta)\sin(\gamma)\sin(\psi)\sin(\delta)\\ &+ \cos(\theta)\sin(\gamma)\cos(\psi)]\\ &+ \mathbf{c}[\cos(\theta)\sin(\psi)\sin(\delta)\\ &- \sin(\theta)\cos(\psi)], \end{aligned} \quad (2)$$

where δ (defined in terms of the transformed axes) takes the values 0–2π to represent different orientations of the POD on the cone around $\mathbf{K}_{hkl}$. A simple vector (dot) product of (1) and (2) then gives

$$\begin{aligned}\cos(\alpha) = \sin(\beta)\cos(\varphi)&[-\sin(\gamma)\sin(\psi)\cos(\delta)\\ &+ \sin(\theta)\cos(\gamma)\sin(\psi)\sin(\delta)\\ &+ \cos(\theta)\cos(\gamma)\cos(\psi)]\\ &+ \sin(\beta)\sin(\varphi)[\cos(\gamma)\sin(\psi)\cos(\delta)\\ &+ \sin(\theta)\sin(\gamma)\sin(\psi)\sin(\delta)\\ &+ \cos(\theta)\sin(\gamma)\cos(\psi)]\\ &+ \cos(\beta)[\cos(\theta)\sin(\psi)\sin(\delta)\\ &- \sin(\theta)\cos(\psi)]. \end{aligned} \quad (3)$$

The ODF is assumed to be a simple function of angle α [here designated $P(\alpha)$], and thus the probability of a crystallite being correctly oriented for diffraction to a particular point on the *hkl* powder ring, $\langle P(\alpha)\rangle_{hkl}$, can be calculated by numerically integrating $P(\alpha)$ over the range of α angles which describe crystallites on the relevant cone. If the ODF is assumed to have the March–Dollase form (March, 1932; Dollase, 1986) then the integral is

$$\begin{aligned}\langle P(\alpha)\rangle_{hkl} = (1/2\pi)\int_0^{2\pi} &[R^{-1}\sin^2(\alpha)\\ &+ R^2\cos^2(\alpha)]^{-3/2}\mathrm{d}\delta, \end{aligned} \quad (4)$$

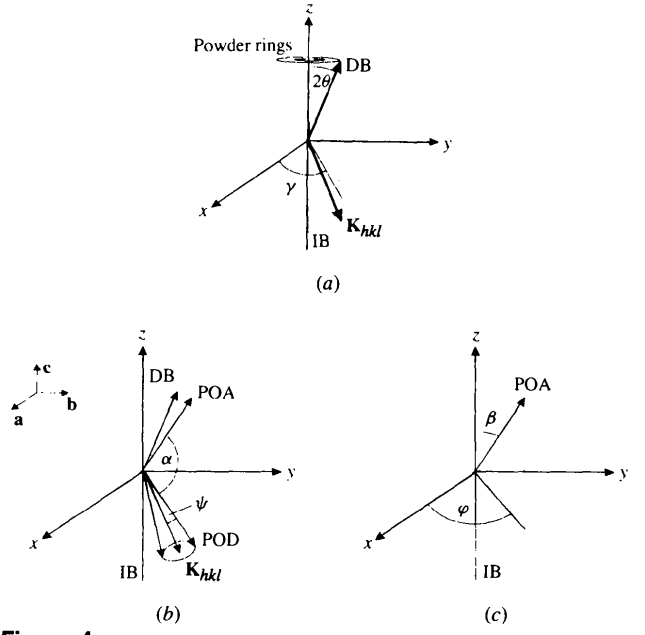

Figure 4
(*a*) The orientation of the incident beam (IB), diffracted beam (DB) and scattering vector ($\mathbf{K}_{hkl}$) with respect to the Cartesian axes. (*b*) The orientation of the PODs with respect to the POA. Angle α describes the orientation of the PODs relative to the POA and thus *varies* for different orientations of the POD on the POD cone around $\mathbf{K}_{hkl}$. ψ is the half-angle of the POD cone. (*c*) The orientation of the POA with respect to the Cartesian axes. Other angles and symbols are defined in the text.

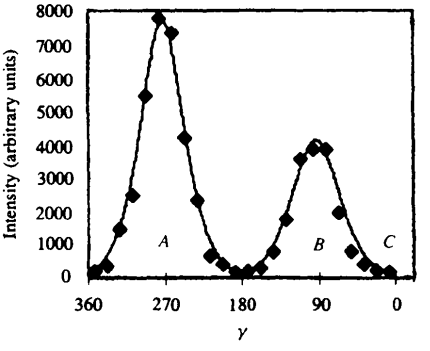

Figure 5
The observed (points) and calculated intensity variation around the powder ring shown in Fig. 1(*b*). The calculated line has been obtained by fitting the preferred-orientation model to the observed data. [The sense of the γ axis is as in Fig. 1.]

where R is the refinable parameter of the March–Dollase function and describes the degree of sample texture. The calculated intensity, $I_{calc}(hkl)$, predicted by the model for that point on the powder ring is then given by:

$$I_{calc}(hkl) = I_{ideal}(hkl) \sum_{M(hkl)} [\langle P(\alpha)\rangle_{hkl}/M(hkl)] \qquad (5)$$

where $I_{ideal}(hkl)$ is the intensity of the (hkl) powder ring from an ideal randomly oriented sample of the same volume, $M(hkl)$ is the multiplicity of the (hkl) reflection and $\langle P(\alpha)\rangle_{hkl}$ is the average value (integrated over the relevant POD cone) of the normalized distribution for that point on the powder ring [from (4)]. The parameters that $\langle P(\alpha)\rangle$ depends on are θ and ψ, which are determined from the lattice parameters and unit-cell indexing; β and φ, the direction of the POA with respect to the incident beam; R, the parameter of the ODF; and γ, the angle around the powder rings. For a given reflection from a given sample in a given orientation, all of these parameters apart from γ are fixed or known. Variation of γ for a given reflection corresponds to the POD cone exploring the ODF, as shown for three different diffracted-beam directions in Fig. 3. [As previously discussed, the variation of intensity with γ is most straightforwardly observed and understood for a single reflection, not overlapped by either symmetry-related reflections or other reflections with almost the same d spacing. However, (5) is summed over all symmetry-related hkl reflections: when applied to the tetragonal sample considered in §2 above, for example, the calculated intensity for the (100) ring as a function of γ will then be the sum of the (100) and (010) variations added together.]

Fig. 5 shows the fit given by the model to the observed intensity around the powder ring of the (non-overlapped) HgS (003) reflection plotted in Fig. 1(*b*). The agreement between the data and the calculated intensity predicted by the model is excellent and indicates that this approach can be used to understand the effects of very pronounced preferred orientation on the full two-dimensional diffraction pattern.

4. Two-dimensional aspects of preferred orientation in some standard geometries

This section discusses the implications of preferred orientation for data collection in the principal standard diffraction geometries used in synchrotron studies.

4.1. *Transmission geometry*

In this case, the incident beam strikes the sample along the axis of the crystallite distribution (the POA) and thus transmission geometry is identical to the simple case considered above in Fig. 3(*a*). This is the diffraction geometry commonly used in high-pressure X-ray studies – assuming the POA to be aligned with the pressure-cell axis as is often, although not always, true. The consequences of this scattering geometry can be seen mathematically in the simplification of (3) when $\beta = 0°$:

$$\cos(\alpha) = \cos(\theta)\sin(\psi)\sin(\delta) - \sin(\theta)\cos(\psi). \qquad (6)$$

i.e. there is no dependence of the value of $\cos(\alpha)$ [and hence $\langle P(\alpha)\rangle_{hkl}$] on the angle around the powder ring, γ. The effects of preferred orientation are seen only in changes to the relative intensities between reflections compared with those obtained from an ideal non-textured sample. The presence of preferred orientation is then not readily apparent and can be detected only if a structural model is available. However, this difficulty can be overcome by inclining the sample such that the X-ray beam strikes the sample at an angle [*i.e.* the general case of Fig. 3(*b*) considered above]. We have found this inclination technique to be of great value as it allows any preferred orientation to be explored prior to structural solution or refinement, and we now routinely apply it to most samples.

4.2. *Debye–Scherrer geometry*

In this geometry the incident beam enters the sample perpendicular to the sample capillary axis, with which the POA is assumed to be coincident (see Fig. 6). For a small ψ angle (as drawn), the POD cones for points A and B in the diffraction pattern are at higher probability than the cone for point C and so point C is a minimum. [As discussed in relation to Fig. 3(*b*), this would be reversed for a reflection with a sufficiently large ψ angle, and C would become a maximum.] As the contours on which the POD cones lie for points A and B are the same, the maxima at points A and B are of equal intensity. It is common during data collection

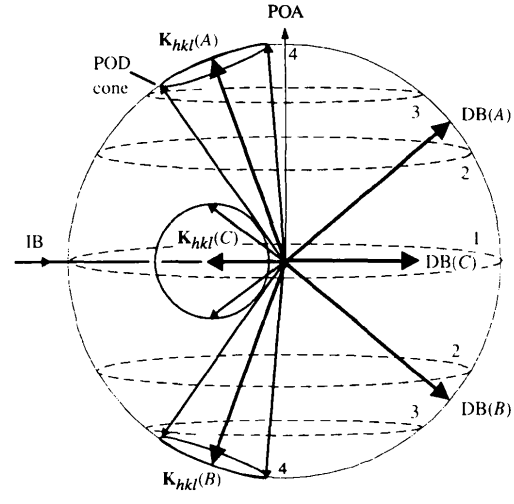

Figure 6
Debye–Scherrer geometry. The orientation of the POD cones for diffraction into three selected points on a powder ring for the incident beam (IB) striking the crystallite distribution perpendicular to the sample capillary axis, which is assumed to be coincident with the POA. By comparing the values of the contours intersected by the POD cones at the three selected points, it can be seen that points A and B are equal relative maxima and point C is a minimum. $\mathbf{K}_{hkl}(C)$ and DB(C) are directed upwards out of the plane of the diagram.

in this geometry to rotate the capillary about its own axis. This enforces the axial symmetry about the POA (which is otherwise only assumed). However, as can be seen from Fig. 6, the variation in intensity around the powder ring is unaffected by this rotation.

This geometry is commonly used with a high-resolution scanning detector, which records a thin strip of the diffraction pattern in the plane perpendicular to the POA. No information on intensity variation around the powder rings is recorded, and hence the presence of preferred orientation cannot be determined unless a structural model is available. However, the degree of preferred orientation could be readily assessed by placing an area detector, such as an image plate, perpendicular to the incident beam so as to record a substantial fraction of the powder rings. Simple averaging of the intensity around the powder rings would produce intensities closer to those expected from a ideal sample than those obtained by the one-dimensional detector, although for optimum accuracy the intensity variation around the powder rings should be modelled and the correct intensities obtained accordingly.

It is possible that the true POA of the sample may not coincide with the capillary axis (as assumed above), or not with the axis around which the capillary is rotated. The rotation will then produce a more complex, albeit still symmetric, effective ODF. In such cases, the maxima at points A and B would remain equal for a rotating sample but would be found to differ in intensity with the sample stationary.

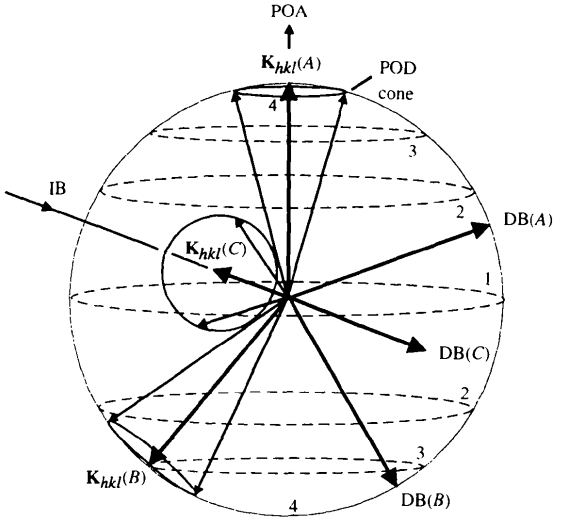

Figure 7
Bragg–Brentano geometry. The orientation of the POD cones for diffraction into three selected points on a powder ring for the incident beam (IB) striking the crystallite distribution such that, for DB(A), the scattering vector $\mathbf{K}_{hkl}$ is coincident with the flat-plate normal (assumed to be coincident with the POA). By comparing the values of the contours intersected by the POD cones at the three selected points, it can be seen that points A and B are unequal relative maxima and point C is a minimum. At point A, the contours intersected by the POD cone are of constant value. $\mathbf{K}_{hkl}(C)$ and DB(C) are directed upwards out of the plane of the diagram.

4.3. *Bragg–Brentano geometry*

In this geometry, the orientation of the sample relative to the incident beam is adjusted for each reflection such that the scattering vectors for the crystallites contributing to the measured intensity coincide with the normal to the flat-plate sample holder. One particular such setting is shown in Fig. 7, with the detector taken to be at point A on the powder ring and the POA assumed to coincide with the flat-plate normal (around which the sample is usually rotated). Points A and B are maxima in the diffraction pattern and point C is a minimum for a reflection with a small POD-cone angle, ψ, as previously discussed. And it can be seen that point A is at a stronger maximum than point B. This geometry is normally used with a small detector [at point A, *i.e.* set to collect DB(A)], and so the intensity variation around the powder rings is not observed. The Bragg–Brentano geometry represents a special case in which measurements are made with all positions on the POD cone lying on the same contour ($\alpha = \psi$), and thus $P(\alpha)$ is the same for all contributing crystallites.

As in the Debye–Scherrer case, the preferred orientation could be readily assessed by taking an exposure with the sample stationary and an image plate placed perpendicular to the incident beam – including, in a similar way, an assessment of the assumption that the POA coincides with the flat-plate normal.

5. Conclusions

We have shown how the detection and modelling of preferred orientation can be greatly aided and simplified by the collection of full two-dimensional powder patterns on a suitable area detector, and have presented a straightforward graphical interpretation of preferred-orientation effects in two-dimensional patterns for a number of standard diffraction geometries. We have also outlined the essential elements of a general quantitative model.

In closing, we remark that a simple *qualitative* assessment of the preferred orientation in a sample can be valuable, and is often sufficient for many purposes. For example, a two-dimensional pattern collected with the incident beam inclined to the expected preferred-orientation axis will reveal immediately whether the sample has any significant preferred orientation and, if so, approximately how strong the effects are. This is already useful information. Beyond that, a comparison of two-dimensional patterns collected at two different inclinations to the preferred-orientation axis will show directly which reflections are weakened and which are strengthened by preferred-orientation effects, and that is sufficient to place tight constraints on any preferred-orientation model included in structure refinement. With a little more effort, but still without quantitative modelling of the two-dimensional data, it is often even possible to identify the preferred-orientation direction using the simple graphical approach we have proposed.

We suggest that many powder diffraction studies would benefit from the routine collection of two-dimensional

patterns to assess sample preferred orientation in these ways – and better still, model it. This is particularly true for work at synchrotron sources where area-detector systems are now becoming widely available and good two-dimensional patterns can be collected very quickly.

This work is supported by the UK Engineering and Physical Sciences Research Council and by facilities made available by Daresbury Laboratory, UK. We are grateful for assistance with the experimental facilities from G. Bushnell-Wye and A. A. Neild.

References

Barrett, C. & Massalski, T. B. (1992). *Structure of Metals, International Series on Materials Science and Technology*, Vol. 35. Oxford: Pergamon Press.

Bunge, H. J., Dahms, M. & Brokmeier, H. G. (1989). *Crystallogr. Rev.* **2**, 67–86.

Capkova, P., Peschar, R. & Schenk, H. (1993). *J. Appl. Cryst.* **26**, 449–452.

Capkova, P. & Valvoda, V. (1974). *Czech. J. Phys.* B**24**, 891–894.

Cerny, R., Valvoda, V. & Chladek, M. (1995). *J. Appl. Cryst.* **28**, 247–253.

Dahms, M. & Bunge, H. J. (1989). *J. Appl. Cryst.* **22**, 439–447.

Dollase, W. A. (1986). *J. Appl. Cryst.* **19**, 267–272.

Järvinen, M. (1993). *J. Appl. Cryst.* **26**, 525–531.

Järvinen, M., Merisalo, M., Pesonen, A. & Inkinen, O. (1970). *J. Appl. Cryst.* **3**, 313–318.

March, A. (1932). *Z. Kristallogr.* **81**, 285–288.

Nelmes, R. J. & McMahon, M. I. (1994). *J. Synchrotron Rad.* **1**, 69–73.

Peschar, R. & Schenk, H. (1995). *J. Appl. Cryst.* **28**, 127–140.

Rietveld, J. (1969). *J. Appl. Cryst.* **2**, 1–8.

Wright, N. G. (1995). PhD thesis, The University of Edinburgh, Scotland.